Stability Enhancement in High-Penetration Wind Power Grid Integration During Fault Conditions Using a Combined MBPSS and FACTS Device Approach

Bilel Dhouib[1], Mohamed Ali Zdiri[1,*] and Hsan Hadj Abdallah[1]

[1]*Control and Energy Management Laboratory, National Engineering School of Sfax, University of Sfax, Sfax* 3038*, Tunisia*

Abstract: This study investigates how a combination of Multi-Band Power System Stabilizers (MBPSS) and Flexible AC Transmission System (FACTS) devices might improve stability in power networks with significant wind energy penetration under fault conditions. Maintaining system stability becomes increasingly important as wind power integration rises, especially when there are disruptions that could cause electromechanical oscillations. The study uses MBPSS to model a wind turbine powered by a Doubly-Fed Induction Generator (DFIG) and assesses the performance of several FACTS devices, including Unified Power Flow Controllers (UPFC), Static Synchronous Series Compensators (SSSC), and Static Synchronous Compensators (STATCOM). According to simulation results, combining these technologies reduces oscillations significantly—for example, damping times decreased from 8 s (without controllers) to 3 s (with MBPSS and UPFC), and frequency deviations were maintained within ±0.5 Hz. These results demonstrate that the UPFC and MBPSS combination is the most effective in stabilizing the grid when wind energy levels are high.

Keywords: Wind Farms, DFIG, UPFC, MBPSS, FACTS, Transient Stability, Power Oscillation Damping, High Wind Penetration.

1. INTRODUCTION

Concerns about climate change and the limited availability of fossil fuels have generated considerable interest in renewable energy as a critical research area for power system stability of study. Renewable sources like wind and solar power present viable alternatives to reduce dependency on traditional fossil fuels. As wind farm installations increase, studies indicate that the reliability and robustness of wind turbines also improve [1, 2]. However, these farms need to align electricity supply with the grid's wind conditions and demand [3].

The extensive integration of intermittent energy sources can challenge power system stability, especially under inadequate control or damping measures. A power system is considered stable if it can maintain equilibrium under normal operations and return to a balanced state after disruptions [4]. Stability issues may arise from factors such as loss of synchronism, low voltage, natural disturbances, or issues in protection systems [5].

Power swings, also known as electromechanical oscillations in generators, are caused by disturbances in a power system and must be effectively dampened to maintain stability. These oscillations are generally classified as follows [6, 7]:

These varied oscillation frequencies have driven the advancement of Multi-Band Power System Stabilizers (MBPSS), which provide suitable damping under different operating conditions [8]. The MBPSS supplies stabilization signals across multiple frequency bands, enhancing system robustness under diverse disturbances.

Research has shown that MBPSS can significantly improve stability in large interconnected grids, such as the New York State power network, through wide-area control strategies [9]. Moreover, discrete mode controllers have been demonstrated to enhance stability in AC microgrids with high renewable integration [10].

In addition to MBPSS, Flexible AC Transmission System (FACTS) devices have attracted attention for their ability to enhance both power transmission capacity and system stability [11]. Studies have demonstrated the effectiveness of FACTS devices such as SSSC and STATCOM in improving resilience after severe faults [12-15]. Furthermore, recent research emphasizes the importance of coordinated control between MBPSS and FACTS devices to strengthen power system stability [16, 17].

This study aims to compare the effectiveness of FACTS devices combined with MBPSS in damping electromechanical oscillations during high-penetration wind power grid integration, particularly under fault conditions. A variable-speed Doubly-Fed Induction Generator (DFIG)-based wind turbine model is developed, incorporating wind dynamics, aerodynamics, and DFIG control. The proposed FACTS-based control methods are then evaluated for their ability to mitigate oscillations under fault conditions and high wind power integration.

*Address correspondence to this author at the Control and Energy Management Laboratory, National Engineering School of Sfax, University of Sfax, Sfax 3038, Tunisia;
E-mail: mohamed-ali.zdiri@enis.tn

Received on 05-08-2025 Accepted on 15-09-2025 Published on 17-09-2025

E-ISSN: 2410-2199/25

Table 1: Classification of Power System Oscillations

Type of Oscillation	Frequency Range	Description
Local oscillations	0.8 – 4.0 Hz	Occur within a unit and the rest of its generating station or larger power system.
Interplant oscillations	1.0 – 2.0 Hz	Appear between two closely related generating plants.
Interarea oscillations	0.2 – 0.8 Hz	Occur between two significant groups of generating plants.
Global oscillations	< 0.2 Hz	Represent synchronous oscillation of all generators in isolated structures.

The principal contributions of this study are as follows:

- Integration of MBPSS with different FACTS devices, including SSSC, STATCOM, and UPFC, to enhance power system stability in scenarios with high levels of wind energy penetration.
- Evaluation of how effectively these control strategies improve the damping of electromechanical oscillations.
- Development of a DFIG-based wind turbine model incorporating wind dynamics and aerodynamic performance, crucial for assessing system response under fault conditions.

The paper is organized as follows: Section 2 examines the system model; Section 3 describes the test system; Section 4 presents simulation results and analysis; and Section 5 provides the study's conclusions.

2. SYSTEM MODELING

Comprehensive discussions on synchronous machine dynamic models appropriate for stability analysis can be found in [18]. This section concentrates on the modeling of DFIG systems. DFIG wind turbines connect to the power grid through power converters, as demonstrated in Figure **1**.

A. Wind Speed Model

The wind speed $V(t)$ can be modeled as a sum of harmonic components [19]:

$$V(t) = A_0 + \sum_{n=1}^{N} A_n * cos(\omega_n t + \phi_n) \quad (1)$$

where $V(t)$ is the wind speed at time t, A_0 is the average wind speed, A_n is the amplitude of the n-th harmonic, ω_n (equal to $2\pi f_n$) is its angular frequency, ϕ_n is the phase shift, and N is the total number of harmonics. This formulation provides a detailed representation of wind speed variations over time, accounting for different frequency influences.

B. Aerodynamic Model

In this study, the aerodynamic model is formulated based on the relationship between wind speed, blade geometry, and aerodynamic forces, which allows for accurate estimation of captured wind power and its impact on DFIG-based wind turbine performance [20].

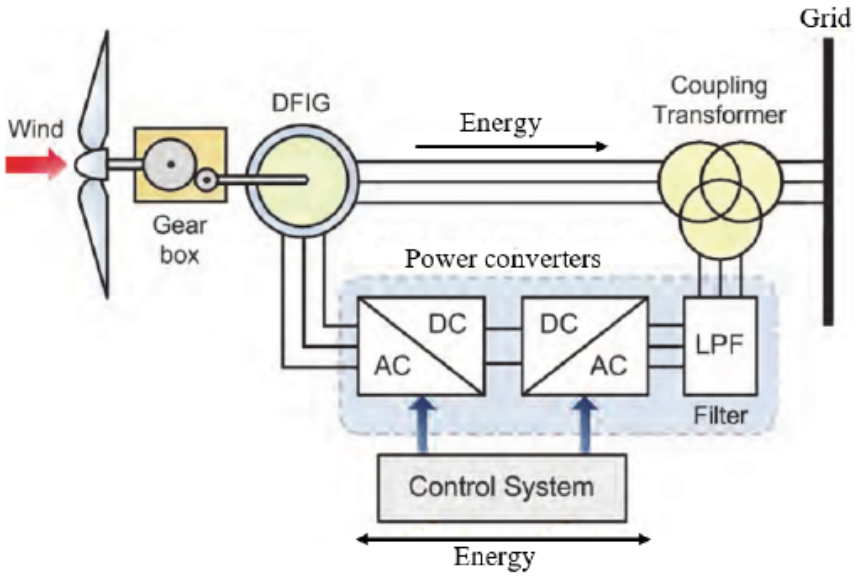

Figure 1: A standard setup for a DFIG wind system connected to the grid.

$$P = \frac{1}{2} * \rho * A * V^3 * C_p(\lambda, \beta) \quad (2)$$

where ρ represents air density, A is the turbine's swept area, V is the wind speed, and C_p is the power coefficient, which depends on the tip-speed ratio λ and the blade pitch angle β.

C. Doubly-Fed Induction Generator Electrical Model

The DFIG is commonly utilized in wind energy systems because of its capacity to manage both active and reactive power while ensuring grid stability. Below is a summary of the DFIG electrical model, highlighting its main components and equations [21].

Stator voltage equations:

$$\begin{cases} v_{ds} = -r_s I_{ds} - \omega_s \Phi_{qs} + \frac{d\Phi_{ds}}{dt} \\ v_{qs} = -r_s I_{qs} + \omega_s \Phi_{ds} + \frac{d\Phi_{qs}}{dt} \end{cases} \quad (3)$$

Rotor voltage equations:

$$\begin{cases} v_{dr} = -r_r I_{dr} - (\omega_s - \omega_r)\Phi_{qr} + \frac{d\Phi_{dr}}{dt} \\ v_{qr} = -r_r I_{qr} + (\omega_s - \omega_r)\Phi_{dr} + \frac{d\Phi_{qr}}{dt} \end{cases} \quad (4)$$

Stator and rotor flux linkages:

$$\begin{cases} \Phi_{ds} = -l_{ls} I_{ds} + l_m (I_{ds} + I_{dr}) \\ \Phi_{qs} = -l_{ls} I_{qs} + l_m (I_{qs} + I_{qr}) \\ \Phi_{dr} = -l_{lr} I_{dr} + l_m (I_{ds} + I_{dr}) \\ \Phi_{qr} = -l_{lr} I_{qr} + l_m (I_{qs} + I_{qr}) \end{cases} \quad (5)$$

Electromagnetic torque equation:

$$C_e = (3/2)(p/2) l_m (I_{qs} I_{dr} - I_{ds} I_{qr}) \quad (6)$$

In this context, v_{ds}, v_{qs}, v_{dr}, and v_{qr} represent the voltages of the stator and rotor, while I_{ds}, I_{qs}, I_{dr}, and I_{qr} denote the respective stator and rotor currents. The flux linkages for both the stator and rotor are represented by Φ_{ds}, Φ_{qs}, Φ_{dr}, and Φ_{qr}. The stator and rotor resistances are indicated by r_s and r_r, with l_{ls} and l_{lr} referring to the leakage inductances. The magnetizing inductance is denoted by l_m, while ω_s and ω_r signify the synchronous and rotor speeds, respectively. Additionally, p represents the number of pole pairs, and C_e denotes the electromagnetic torque.

The DFIG electrical model represents the critical dynamics of the generator and its connection to the grid. By integrating rotor and stator equations, power computations, and control strategies, the DFIG effectively handles fluctuating wind conditions while ensuring stable operation and maintaining power quality. This adaptability is why it is a favored option in contemporary wind energy systems.

D. Multi-Band Power System Stabilizers Model

By employing numerous frequency bands, the MBPSS is intended to improve damping over a broad range of electromechanical oscillation frequencies. A low-frequency band to reduce global oscillations (less than 0.2 Hz), an intermediate-frequency band to handle inter-area oscillations (0.2–0.8 Hz), and a high-frequency band to suppress local oscillations (0.8–4 Hz) are the three bands that are usually included in its structure. A phase compensation network, a band-pass filter, and a gain make up each band [22].

After passing through a limiter, the MBPSS output—which is the total of the stabilizing signals from various bands—is supplied to the generator's excitation system. The following is the expression for the MBPSS's general transfer function:

$$V_{ST}(s) = \sum_{i=1}^{3} K_i \cdot \frac{T_{1i}s+1}{T_{2i}s+1} \cdot \frac{T_{3i}s}{T_{4i}s+1} \cdot \Delta\omega(s) \quad (7)$$

where $V_{ST}(s)$ is the stabilizer output, $\Delta\omega(s)$ is the rotor speed deviation input, K_i is the stabilizer gain, and T_{1i}, T_{2i}, T_{3i}, and T_{4i} are time constants associated with the lead–lag compensators and band-pass filters.

The MBPSS uses the three frequency-selective channels to process the rotor speed variation, as shown in Figure **2**. The MBPSS enhances transient and dynamic stability by offering suitable phase compensation and damping torque, guaranteeing efficient oscillation suppression under a range of operating circumstances.

E. Static Synchronous Series Compensators Model

The SSSC is modeled as a series-connected voltage source, labeled $\bar{\vartheta}_s$, as shown in Figure **3**. This voltage consistently remains in quadrature with the line current, meaning it is perpendicular in phase. As a result, only the magnitude of $\bar{\vartheta}_s$ can be controlled [23].

The total active and reactive power flows in a transmission line with an SSSC are as follows [24]:

$$\begin{cases} P_{Km} = (1+\varepsilon)\frac{V_K V_m}{x\, K_m} sin(\theta_K - \theta_m) \\ P_{mK} = -P_{Km} \\ Q_{Km} = (1+\varepsilon)\frac{V_K}{x\, K_m}(V_K - V_m\, cos(\theta_K - \theta_m)) \\ Q_{mK} = (1+\varepsilon)\frac{V_m}{x\, K_m}(V_m - V_K\, cos(\theta_K - \theta_m)) \end{cases} \quad (8)$$

With:

$$\varepsilon = \frac{v_S}{\sqrt{V_K^2 + V_m^2 - 2V_K V_m\, cos\, \theta_{Km}}}$$

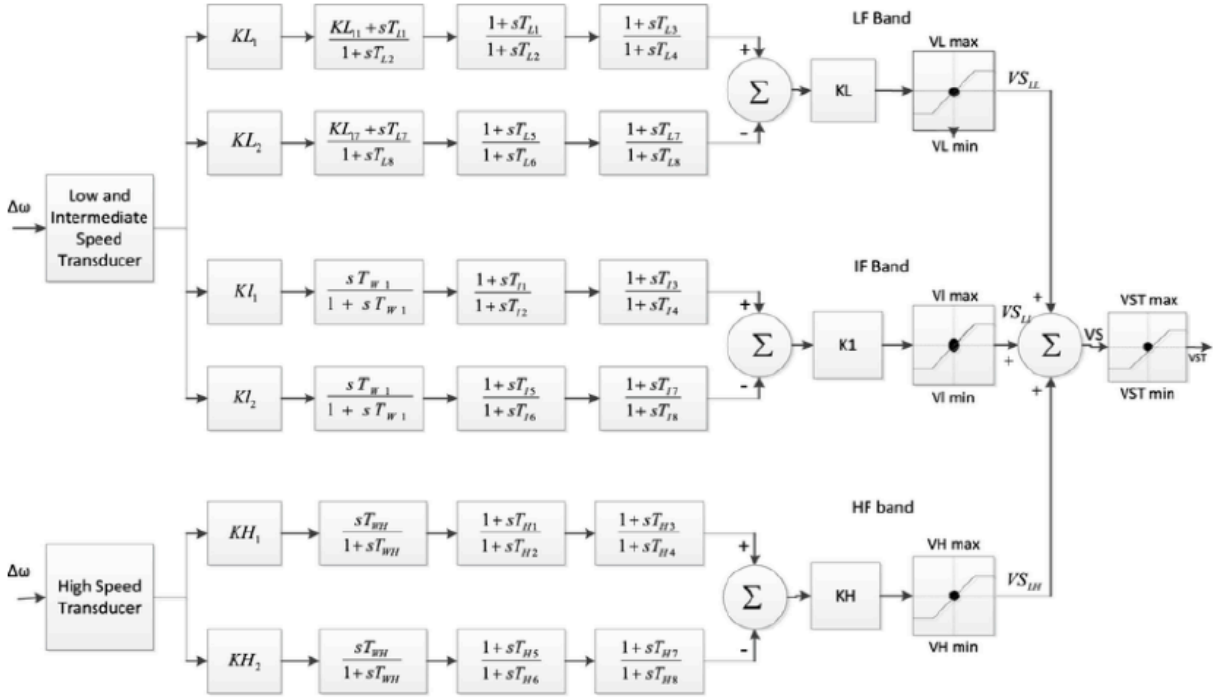

Figure 2: MBPSS circuit model.

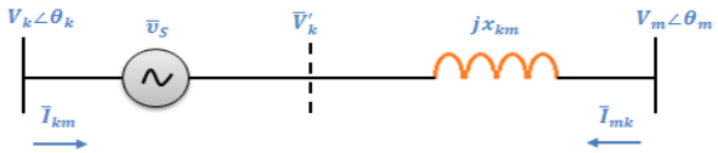

Figure 3: SSSC circuit model.

F. Static Synchronous Compensators Model

In this implementation, the STATCOM model operates as a current injection model, in which the AC system and the STATCOM solely exchange reactive power. This is accomplished by keeping the STATCOM current and bus voltage in quadrature. In Figure **4**, the dynamic model is displayed [25].

The differential equation and the reactive power injected at the STATCOM node are expressed as follows [26]:

$$\bar{\imath}_{SH} = \left(K_r\left(V_{ref} + \upsilon_{POD} - V\right) - \bar{\imath}_{SH}\right)/T_r \tag{9}$$

$$Q = -\bar{\imath}_{SH}V \tag{10}$$

G. Unified Power Flow Controllers Model

The UPFC circuit model combines components from both the STATCOM and the SSSC. It is represented by a series voltage source, $\bar{v}_S$ and a shunt current source, $\bar{\imath}_{SH}$ as shown in Figure **5** [27].

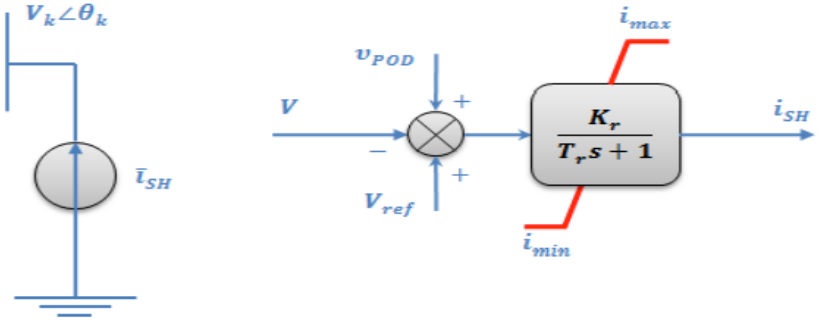

Figure 4: Circuit model and control block diagram of STATCOM.

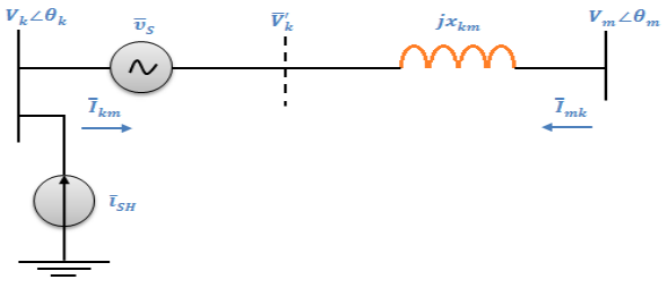

Figure 5: UPFC circuit model.

These sources are defined as follows [28]:

$$\begin{cases} \bar{v}_S = (v_p + v_q)e^{j\phi} = r\bar{V}_K e^{j\gamma} \\ \bar{\imath}_{SH} = (i_p + i_q)e^{j\theta_K} \end{cases} \quad (11)$$

The UPFC power injection model describes its influence on the power system as active and reactive power injected at the respective buses. The equations governing power injection for this model are:

$$\begin{cases} P_{Km} = b_r V_K V_m \sin(\gamma + \theta_K - \theta_m) \\ Q_{Km} = b_r V_K^2 \cos\gamma - i_q V_K \\ P_{mK} = -b_r V_K V_m \sin(\gamma + \theta_K - \theta_m) \\ Q_{mK} = -b_r V_K V_m \cos(\gamma + \theta_K - \theta_m) \end{cases} \quad (12)$$

H. Comparative Summary of FACTS Devices

A comparative overview makes clear the different roles that the SSSC, STATCOM, and UPFC play in enhancing power system stability, even if their respective models offer in-depth insights into their dynamic behavior. Due to its series connection, the SSSC mainly uses quadrature voltage injection to regulate the effective line reactance, which enhances power transmission capacity and helps to reduce oscillations. As a shunt-connected device, the STATCOM provides quick dynamic voltage support and enhanced damping performance by exchanging reactive power with the system to control bus voltage. The most adaptable device is the UPFC, which combines shunt and series converters via a single DC link and can simultaneously change line impedance, phase angle, and voltage magnitude. The UPFC is particularly good at reducing electromechanical oscillations and improving transient stability under high renewable penetration because of its multifunctionality.

Table **2** provides a succinct comparison of various FACTS devices' key characteristics.

3. OVERVIEW OF THE TEST NETWORK

A. Western System Coordinating Council System

A simplified version of the Western System Coordinating Council (WSCC) system is modeled by the nine-bus, three-machine test network utilized in the simulations, as shown in Figure **6**. It comprises generators at nodes 1, 2, and 3, rated at 247.5 MVA, 192 MVA, and 128 MVA, respectively, and operates at voltage levels of 16.5 kV, 18 kV, 13.8 kV, and 230 kV. Generator G1 is connected to slack bus 1, while G2 and G3 connect to busbars 2 and 3. The network has six transmission lines and load nodes A, B, and C at busbars 5, 6, and 8, drawing a combined 315 MW. The IEEE 3-machine, 9-bus layout in Figure **6** and the synchronous generator parameters in 'per unit' (Table **3** in Appendix) complete the setup, with each generator featuring standard voltage and speed regulators.

B. Modified Western System Coordinating Council Network

This section examines integrating a wind energy system into the modified 9-bus, three-machine test network to find the optimal turbine integration rate. The network includes two wind farms at bus 7 and bus 9, each with 37 turbines of 1.5 MW, totaling 111 MW and representing a 35% penetration of the 567.5 MW network output. The turbines use DFIG technology, and FACTS devices are placed at bus 8. This location was selected because it is electrically close to both the wind farm integration buses (7 and 9) and a major load

Table 2: Comparison of FACTS Device Models

Device	Connection Type	Control Variable(s)	Primary Role
SSSC	Series	Injected quadrature voltage	Controls line reactance, improves power transfer capability, enhances damping
STATCOM	Shunt	Reactive current injection	Provides fast dynamic voltage support, enhances damping of oscillations
UPFC	Series + Shunt	Series voltage & shunt current	Controls voltage, phase, and impedance simultaneously; most effective for stability and damping

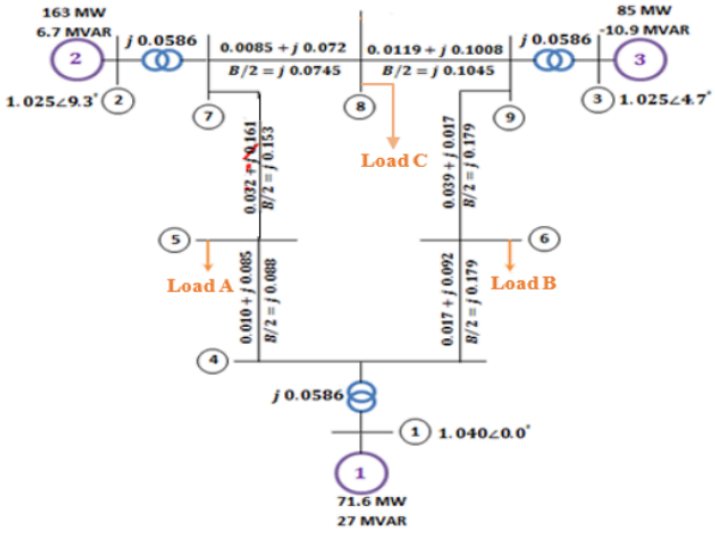

Figure 6: WSCC network.

bus (C), making it a sensitive point for voltage stability and power flow regulation. Placing the devices here maximizes their impact on damping oscillations and enhancing transient stability, consistent with established FACTS allocation practices [20]. An updated grid layout is depicted in Figure **7**. The associated turbine data, expressed in per-unit values, can be found in Tables **4** to **6** in the Appendix. The study specifically investigates the impact of wind power on the system's transient stability.

To determine the optimal turbine integration rate, we adopted an incremental simulation-based methodology. The number of DFIG-based wind turbines connected to the modified WSCC 9-bus network was gradually increased, while monitoring key stability indicators such as rotor angle deviation, angular speed, and system frequency. The integration level at which instability (loss of synchronism, divergence in rotor angles, or unacceptable frequency deviations) first occurred was considered the critical penetration limit. The optimal integration rate was thus defined as the maximum penetration level that maintained stable operation under these conditions. In this study, stability was ensured up to 111 MW (74 turbines), corresponding to approximately 35% of the total network output. This approach is consistent with methodologies reported in earlier works on defining wind power integration limits [3, 20].

4. RESULTS AND DISCUSSIONS

Under load condition C, a three-line to-ground (LLLG) fault was simulated at bus 8. The issue was started at t = 0.5 s and fixed at t = 0.6 s, 100 ms later. The system's transient stability was greatly damaged

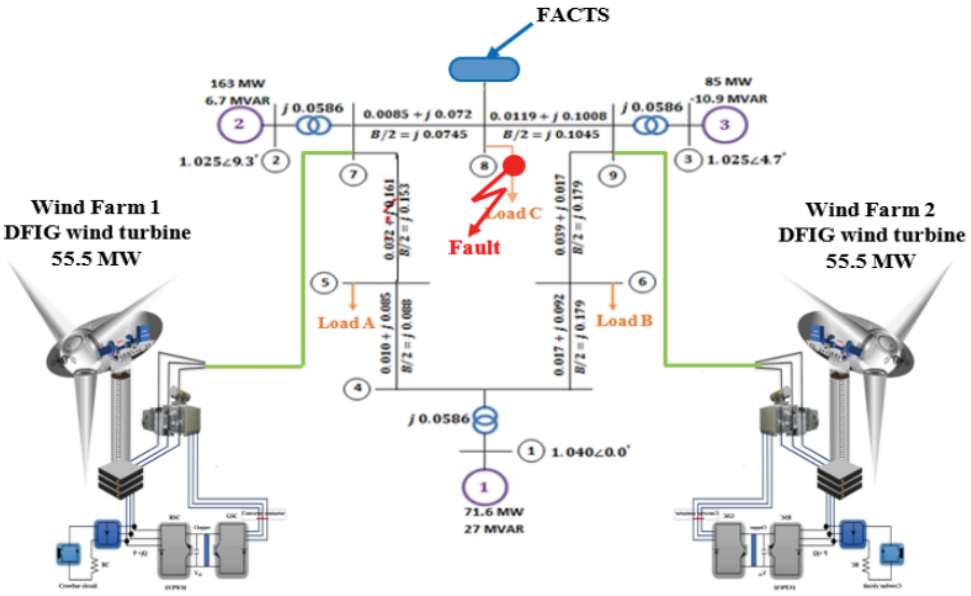

Figure 7: Modified WSSC network.

by this extreme disturbance in addition to the substantial (35%) penetration of wind energy. The power angle and angular speed disparities across generators (δ_{21}, δ_{31}, ω_{21}, ω_{31}) and the frequency at each synchronous generator bus were analyzed in order to assess the performance.

To precisely capture the system dynamics during the fault transient, the simulations were carried out in MATLAB/Simulink R2020a using the ode23tb (stiff/TR-BDF2) solver with a variable step size and a maximum step of 10 ms. A varied wind profile with speeds ranging from 8 to 14 m/s over an 8-second simulation period was used to simulate realistic wind conditions (Figure **8**).

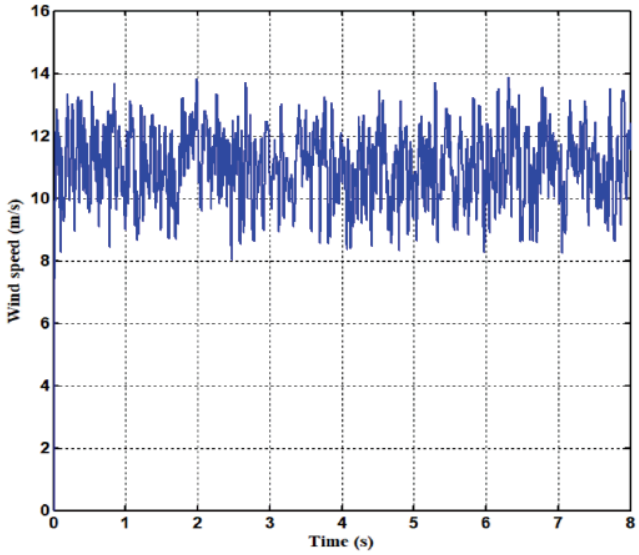

Figure 8: Wind speed variation profile.

The system response was analyzed across four distinct cases:

- Case 1: No controller (Base Case).
- Case 2: MBPSS with SSSC.
- Case 3: MBPSS with STATCOM.
- Case 4: MBPSS with UPFC.

Key quantitative measures such as settling time (time to get within ±2% of steady-state), maximum overshoot, and frequency nadir (lowest frequency point post-fault) for the essential inter-machine rotor angle difference δ_{21} are presented in Table **7**, which summarizes the comparative performance. The table also calculates the percentage improvement for each metric compared to the base case (no controller), clearly demonstrating the superior performance of the coordinated MBPSS-UPFC approach.

Figures **9** through **12** show the time-domain responses of the rotor angle differences (δ_{21}, δ_{31}) and speed differences (ω_{21} , ω_{31}). The findings unequivocally show that the MBPSS-UPFC combination damped electromechanical oscillations the fastest and most efficiently. There are sustained oscillations with amplitudes exceeding 20° in the base case in the base case (no controller). Despite providing dampening, the MBPSS-SSSC design performs poorly, exhibiting a an overshoot of 28.5° in rotor angle deviation of 28.5° and a lengthy settling time of 4.5 s. By lowering the overshoot to 22.1° and the settling time to 4.0 s, the MBPSS-STATCOM pairing demonstrates a noticeable improvement. The MBPSS-UPFC controller, on the other hand, performs better, demonstrating its resilience by reaching stability in just 3.0 seconds with a low overshoot of 18.7°.

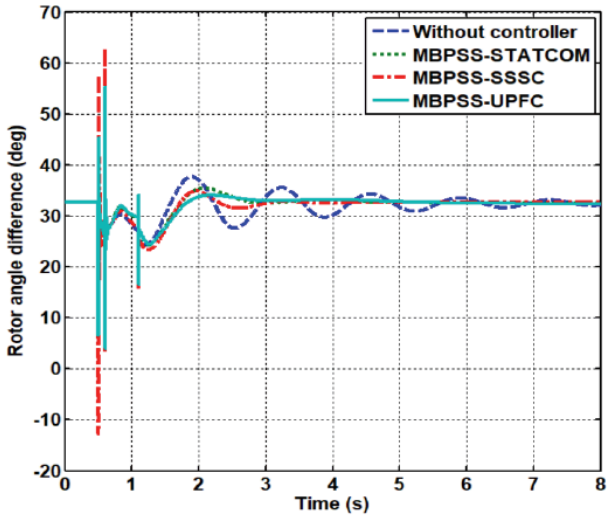

Figure 9: Difference in rotor angle, denoted as δ_{21}.

Table 7: Comparative Performance of Damping Control Strategies

Metric	No Controller	MBPSS-SSSC	MBPSS-STATCOM	MBPSS-UPFC
Settling Time for δ_{21} (s)	> 8.0	4.5	4.0	3.0
Improvement	—	43.8%	50.0%	≥62.5%
Max Overshoot of δ_{21} (deg)	45.2	28.5	22.1	18.7
Improvement	—	36.9%	51.1%	58.6%
Frequency Nadir (Hz)	48.9	49.2	49.4	49.5
Improvement	—	+0.3 Hz	+0.5 Hz	+0.6 Hz

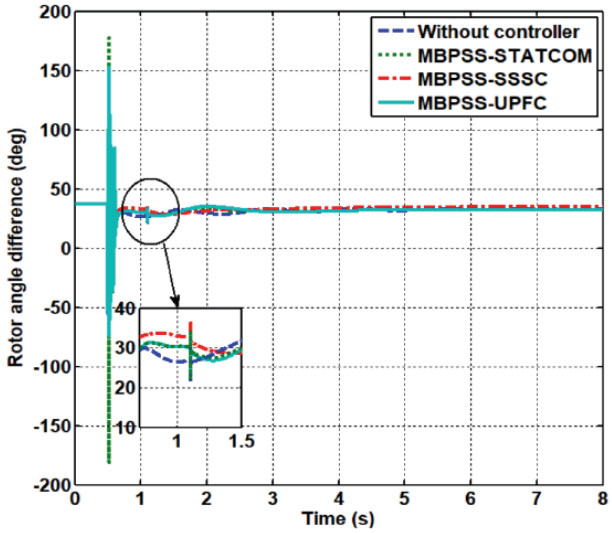

Figure 10: Difference in rotor angle, denoted as δ_{31}.

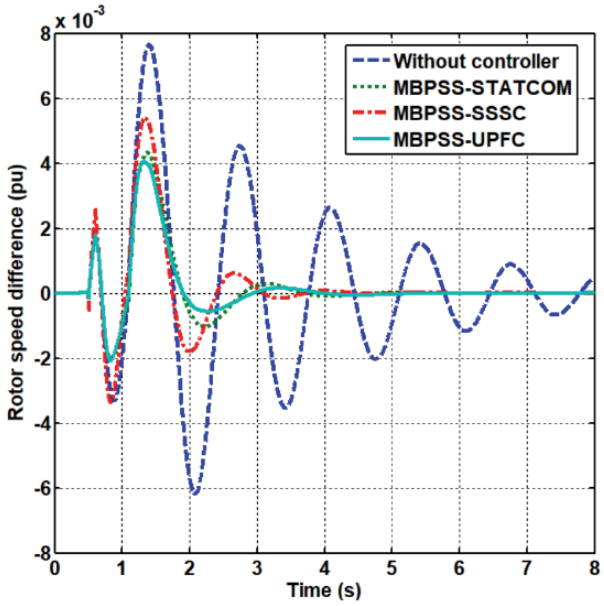

Figure 11: Difference in rotor speed, represented as ω_{21}.

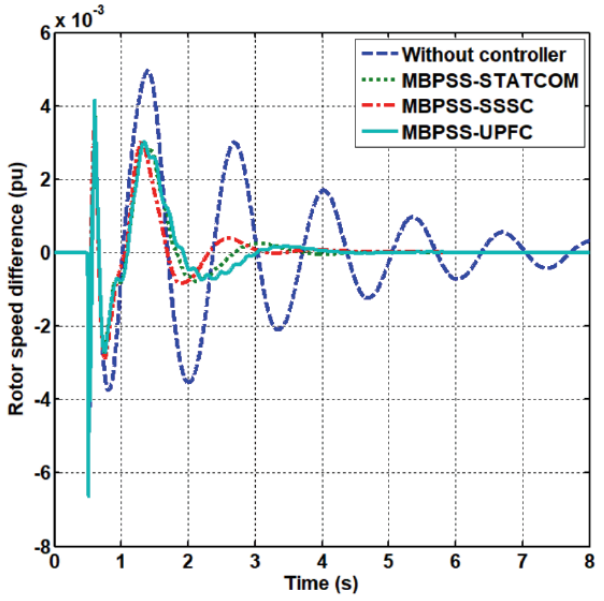

Figure 12: Difference in rotor speed, represented as ω_{31}.

These results are further supported by the network frequency response at each generator bus (Figures **13** to **15**). By limiting the post-fault swing between 50.3 Hz and 49.5 Hz and reaching the greatest frequency nadir of 49.5 Hz, the MBPSS-UPFC combination successfully reduced frequency deviations. Comparing this to the basic case nadir of 48.9 Hz, there is a noticeable improvement. Superior reactive power management and voltage support are made possible by the UPFC's simultaneous and coordinated shunt and series compensation, which is essential for preserving frequency stability both during and after the incident.

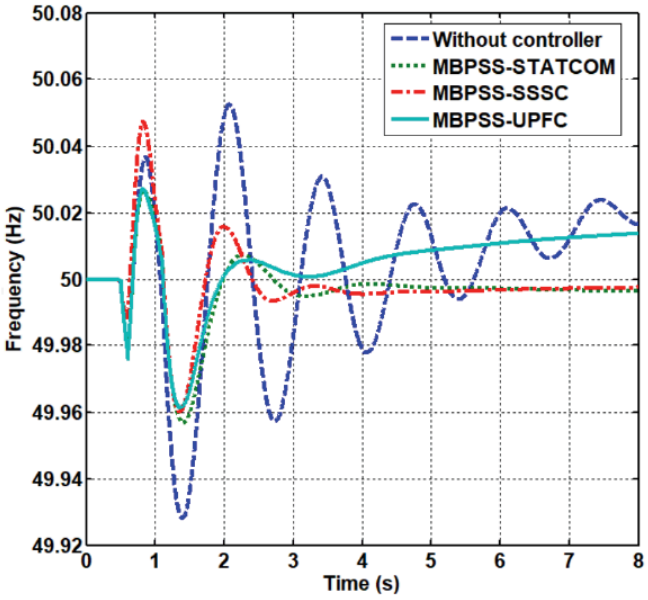

Figure 13: Frequency response of machine 1.

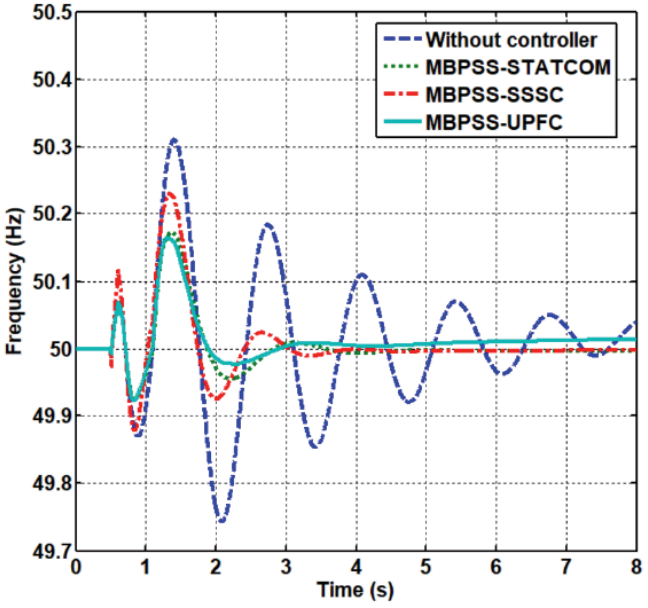

Figure 14: Frequency response of machine 2.

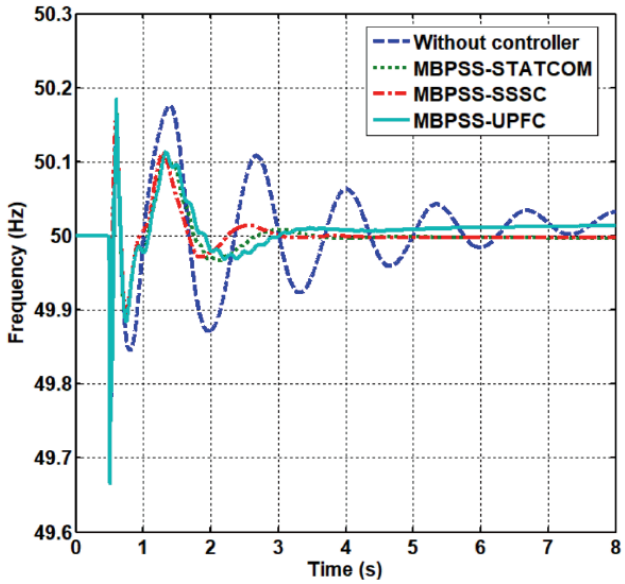

Figure 15: Frequency response of machine 3.

In summary, the simulation findings, which are corroborated by the numerical data in Table **7**, highlight how much more reliable and efficient the UPFC controller in conjunction with MBPSS is than alternatives based on SSSC or STATCOM. Under extreme fault situations and strong wind energy integration, the MBPSS-UPFC design ensures quick convergence to a stable equilibrium with the fastest settling time (3.0 s), the smallest overshoot (18.7°), and the greatest frequency nadir (49.5 Hz).

5. CONCLUSION

This study showed how crucial coordinated control measures are to improving power system stability in the face of severe fault situations and substantial wind energy penetration. While Multi-Band Power System Stabilizers (MBPSS) enhanced damping performance when integrated with any FACTS device, the synergistic coupling of MBPSS and a Unified Power Flow Controller (UPFC) was particularly successful, according to simulations conducted on a modified WSCC network. By quickly reducing electromechanical oscillations, reducing rotor angle overshoot to 18.7 degrees, and keeping frequency within a small range of 49.5–50.5 Hz, this arrangement produced greater transient stability and made it possible to safely integrate a 35% wind power share.

However, this study has several limitations that should be addressed. Although illustrative, the research was carried out on a benchmark nine-bus system, which might not adequately represent the intricate dynamics and scalability issues of larger, actual linked electrical grids. Additionally, even if they are representative, the fault scenario and wind speed profile represent a particular use case. A broader range of operational uncertainties, such as different fault types, locations, and stochastic wind patterns, must be used to validate the performance of the suggested MBPSS-UPFC method.

Future research will therefore concentrate on a few important areas. The main goal is to evaluate scalability by validating these results on bigger, more realistic test systems, like the IEEE 39-bus or 118-bus networks. In order to optimize the real-time tuning of the MBPSS and UPFC parameters in response to shifting system conditions, future research will also investigate the creation and application of an advanced, intelligent coordination mechanism, possibly utilizing artificial intelligence or adaptive control techniques. Lastly, this coordinated solution's transformation from a theoretical idea to a grid-ready technology will require examining its actual deployment hurdles and economic feasibility.

CONFLICTS OF INTEREST

The author declared no conflicts of interest.

Appendix

Table **3** summarizes the synchronous generator parameters used in the WSCC test system, expressed in per unit values for consistency.

Table 3: Synchronous Generator Parameters for the WSCC Test System

Variables	Description	Machine 1	Machine 2	Machine 3	Unit
S	Rated apparent power	247.5×10^6	192×10^6	128×10^6	VA
X_d	Direct-axis synchronous reactance	0.146	0.8958	1.3125	pu
X'_d	Direct-axis transient reactance	0.0608	0.1198	0.1813	pu
X''_d	Direct-axis subtransient reactance	0.0483	0.0891	0.1072	pu
X_q	Quadrature-axis synchronous reactance	0.0969	0.8645	1.2587	pu
X'_q	Quadrature -axis transient reactance	0.0969	0.1198	0.1813	pu

X''_q	Quadrature-axis subtransient reactance	0.0483	0.0891	0.1072	pu
T'_{d0}	Direct-axis transient open-circuit time constant	8.96	6	5.89	s
T''_{d0}	Direct-axis subtransient open-circuit time constant	0.04	0.033	0.033	s
T'_{q0}	Quadrature -axis transient open-circuit time constant	0.31	0.535	0.6	s
T''_{q0}	Quadrature -axis subtransient open-circuit time constant	0.060	0.08	0.07	s
H	Inertia constant	23,64	6,4	3,01	s

Table **4** presents the electrical and mechanical parameters of the DFIG model implemented in the wind turbine simulations.

Table 4: Data related to DFIG

Variables	Description	Values	Unit
S_{nom}	Rated power	1.5/0.9	MVA
V_{nom}	Rated Voltage	0.575×10^{3}	KV
F	Frequency	50	Hz
R_s	Stator Resistance	7.06×10^{-3}	pu
LI_s	Stator Leakage Inductance	17.1×10^{-2}	pu
R'_r	Rotor Resistance	$5\times\ 10^{-3}$	pu
LI'_r	Rotor Leakage Inductance	15.6×10^{-2}	pu
L_m	Magnetizing Inductance	29×10^{-1}	pu
H	Inertia Constant	$504\times\ 10^{-2}$	s
p	Number of Pole Pairs	3	-

Table **5** provides the main turbine specifications, including mechanical output power and pitch control characteristics.

Table 5: Data Related to Turbine

Variables	Description	Values	Unit
$P_{méc\_nom}$	Nominal wind turbine mechanical output power	1.5×10^{6}	W
K_p	Pitch angle controller gain	500	-
β	Maximum pitch angle	49.9	degree

Table **6** lists the converter parameters applied in the simulation model, which govern the dynamic response of the grid-side and machine-side converters.

Table 6: Data Related to Converters

Variables	Description	Values	Unit
P_{max}	Converter maximum power	0.5	pu
$[R\ \ L]$	Grid-side coupling inductor	$[15\times10^{-4}\ 15\times10^{-2}]$	pu
$[\varphi_{Il}\ \ Il]$	Coupling inductor initial current	[90 0]	[degree pu]
V_{dc}	Nominal DC bus voltage	1200	V
C	DC bus capacitor	0.01	F

REFERENCES

[1] Elsharnoby, M. A., El-Banna, S. H., & Helmi, D. H. (2024). Maintaining system stability with high penetration of wind energy via fault ride through (FRT) criteria development (system operator perspective). International Journal of Renewable Energy Research (IJRER), *14*(4), 867-878.

[2] Aldossary, Y. M., Hewahi, N., & Alasaadi, A. (2023). Wind speed forecasting based on data decomposition and deep learning models: A case study of a wind farm in Saudi Arabia.

International Journal of Renewable Energy Research (IJRER), *13*(3), 1285-1296.

[3] Gautam, D., Vittal, V., & Harbour, T. (2009). Impact of increased penetration of DFIG-based wind turbine generators on transient and small signal stability of power systems. IEEE Transactions on Power Systems, *24*(3), 1426-1434. https://doi.org/10.1109/TPWRS.2009.2021234

[4] Abdulraheem, B. S., & Gan, C. K. (2016). Power system frequency stability and control: A survey. International Journal of Applied Engineering Research, *11*(8), 5688-5695.

[5] Mehdipour, C., Hajizadeh, A., & Mehdipour, I. (2016). Dynamic modeling and control of DFIG-based wind turbines under balanced network conditions. International Journal of Electrical Power & Energy Systems, *83*, 560-569. https://doi.org/10.1016/j.ijepes.2016.04.046

[6] Ifanda, I., Rostyono, D., Wijayanto, R. P., Hesty, N. W., Aziz, A., Fauziah, K., ... & Fudholi, A. (2023). Optimizing turbine siting and wind farm layout in Indonesia. International Journal of Renewable Energy Research (IJRER), *13*(3), 1351-1363.

[7] Heniche, A., & Kamwa, I. (2002). Control loops selection to damp inter-area oscillations of electrical networks. IEEE Transactions on Power Systems, *17*(2), 378-384. https://doi.org/10.1109/TPWRS.2002.1007907

[8] Bhadu, M., Punia, V. S., Bishnoi, S. K., & Rathor, B. (2017, October). Robust noise mitigation control techniques for SMIB power system. In 2017 International Conference on Computing and Communication Technologies for Smart Nation (IC3TSN) (pp. 7-12). IEEE. https://doi.org/10.1109/IC3TSN.2017.8284441

[9] Rimorov, D., Heniche, A., Kamwa, I., Babaei, S., Stefopolous, G., & Fardanesh, B. (2017). Dynamic performance improvement of New York state power grid with multi-functional multi-band power system stabiliser-based wide-area control. IET Generation, Transmission & Distribution, *11*(18), 4537-4545. https://doi.org/10.1049/iet-gtd.2017.0288

[10] Arora, A., Bhadu, M., & Kumar, A. (2023, March). Stability enhancement of AC microgrid using discrete mode controllers with optimum sampling frequency. In International Conference on Renewable Power (pp. 943-962). Singapore: Springer Nature Singapore. https://doi.org/10.1007/978-981-99-6749-0_64

[11] Gupta, P. (2015). Damping of power system oscillations using facts devices (Doctoral dissertation, JC Bose University).

[12] Ayres, H. M., Kopcak, I., Castro, M. S., Milano, F., & da Costa, V. F. (2010). A didactic procedure for designing power oscillation dampers of FACTS devices. Simulation Modelling Practice and Theory, *18*(6), 896-909. https://doi.org/10.1016/j.simpat.2010.02.007

[13] Taheri, H., Shahabi, S., Taheri, S., & Gholami, A. (2009, May). Application of synchronous static series compensator (SSSC) on enhancement of voltage stability and power oscillation damping. In IEEE EUROCON 2009 (pp. 533-539). IEEE. https://doi.org/10.1109/EURCON.2009.5167683

[14] Yarlagadda, V., Devulal, B., Kumar, C. S., Ambati, G., Jalluri, S. R., & Garikapati, A. K. (2024). Influence of hybrid FACTS device and STATCOM on power quality improvement of wind farm. Journal of Electrical Systems, *20*(10s), 104-115.

[15] Nayeripour, M., Narimani, M. R., Niknam, T., & Jam, S. (2011). Design of sliding mode controller for UPFC to improve power oscillation damping. Applied Soft Computing, *11*(8), 4766-4772. https://doi.org/10.1016/j.asoc.2011.07.006

[16] Lemdani, S., Laouer, M., & Allali, A. (2019). Stability improvement of power system using a coordinated systems FACTS-PSS, FACTS-MBPSS. International Journal of Systems and Software Engineering (IJSSP), *13*.

[17] Tiwari, A. K., Singh, M., Ralhan, S., & Sahu, N. (2021). Performance analysis of power system stability of four-machine system by using MBPSS and static compensator. In Intelligent Systems: Proceedings of SCIS 2021 (pp. 29-38). Springer Singapore. https://doi.org/10.1007/978-981-16-2248-9_4

[18] Kundur, P. (2007). Power system stability. In Power System Stability and Control (pp. 7-1). McGraw-Hill. https://doi.org/10.1201/9781420009248.sec2

[19] Zdiri, M. A., Dhouib, B., Alaas, Z., & Hadj Abdallah, H. (2023). A low-voltage AC, low-voltage DC, and high-voltage DC power distribution system with grid: Design and analysis. Applied Sciences, *13*(2), 808. https://doi.org/10.3390/app13020808

[20] Dhouib, B., Alaas, Z., Kahouli, O., & Haj Abdallah, H. (2020). Determination of optimal location of FACTS device to improve integration rate of wind energy in presence of MBPSS regulator. IET Renewable Power Generation, *14*(17), 3526-3540. https://doi.org/10.1049/iet-rpg.2020.0679

[21] Dhouib, B., Zdiri, M. A., Alaas, Z., & Hadj Abdallah, H. (2023). Fault analysis of a small PV/wind farm hybrid system connected to the grid. Applied Sciences, *13*(3), 1743. https://doi.org/10.3390/app13031743

[22] Kumkratug, P., & Haque, M. H. (2003, July). Improvement of stability region and damping of a power system by using SSSC. In 2003 IEEE Power Engineering Society General Meeting (IEEE Cat. No. 03CH37491) (Vol. 3). IEEE.

[23] Mihalic, R., & Gabrijel, U. (2004). A structure-preserving energy function for a static series synchronous compensator. IEEE Transactions on Power Systems, *19*(3), 1501-1507. https://doi.org/10.1109/TPWRS.2004.826767

[24] Rahim, A. H. M. A., Al-Baiyat, S. A., & Al-Maghrabi, H. M. (2002). Robust damping controller design for a static compensator. IEE Proceedings-Generation, Transmission and Distribution, *149*(4), 491-496. https://doi.org/10.1049/ip-gtd:20020344

[25] Haque, M. H. (2004). Improvement of first swing stability limit by utilizing full benefit of shunt FACTS devices. IEEE Transactions on Power Systems, *19*(4), 1894-1902. https://doi.org/10.1109/TPWRS.2004.836243

[26] Meng, Z. J., & So, P. L. (2000, January). A current injection UPFC model for enhancing power system dynamic performance. In 2000 IEEE Power Engineering Society Winter Meeting. Conference Proceedings (Cat. No. 00CH37077) (Vol. 2, pp. 1544-1549). IEEE. https://doi.org/10.1109/PESW.2000.850212

[27] Kumkratug, P., & Haque, M. H. (2003). Versatile model of a unified power flow controller in a simple power system. IEE Proceedings-Generation, Transmission and Distribution, *150*(2), 155-161. https://doi.org/10.1049/ip-gtd:20030094

[28] Kumkratug, P., & Haque, M. H. (2003). Versatile model of a unified power flow controller in a simple power system. IEE Proceedings-Generation, Transmission and Distribution, 150(2), 155-161. https://doi.org/10.1049/ip-gtd:20030094

https://doi.org/10.31875/2410-2199.2025.12.07